Heliyon 10 (2024) e31833

Contents lists available at ScienceDirect

Heliyon

journal homepage: www.cell.com/heliyon

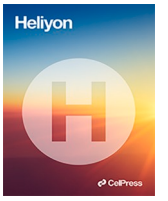

Research article

# Finite element analysis of a generalized rotating FGM vessel subjected to thermo-mechanical loadings: Effect of Poisson ratio and inhomogeneity parameters

P. Das [a,b], A. Benslimane [c,*], M.A. Islam [a], A.A. Siddiquei [b], M.M. Rahman [b], Md Mahmudul Adil [a,b]

[a] Department of Mechanical Engineering, Khulna University of Engineering & Technology, Khulna, 9203, Bangladesh
[b] Department of Mechanical Engineering, Bangladesh Army University of Science and Technology, Saidpur, Bangladesh
[c] Laboratoire de Mécanique, Matériaux et Energétique, Université de Bejaia, Targa Ouzemmour, Bejaia, 06000, Algeria

ARTICLE INFO

*Keywords:*
Generalized functionally graded material (G-FGM)
Finite element analysis (FEA)
Thermo-elasticity
Thick-walled rotating pressure vessel
Variable Poisson ratio

ABSTRACT

Cylinders and thick walled cylindrical shells are commonly utilized in several industries to transport and store fluids under certain pressure and temperature conditions. In the present paper, a numerical solution is developed in order to investigate displacement, temperature and stress fields in a rotating pressure vessel made of generalized functionally graded material (FGM) subjected to different thermo-mechanical boundary conditions. The aim is to investigate the effect of Poisson ratio, internal pressure and temperature and inhomogeneity parameters on the stress and deformation distributions of the rotating pressure vessel. The material is considered isotropic nonhomogeneous and linearly elastic with its properties varying along the radial direction. Additionally, certain conditions, such as exterior or interior problems where $r \to \infty$ or $r \to 0$, respectively, are impossible to resolve using the variation of attributes as a power-law distribution. An approach to the spatial Young modulus distribution that is more broad has been suggested in the literature which can be applied to such physical challenges. The rotation of the pressure vessel is considered in the analysis, and the temperature distribution is assumed to be non-uniform. Since an analytical solution to the differential equation is not accessible, the conventional Galerkin discretization approach of the Finite Element Method (FEM) is applied, nowadays is considered one of the main numerical tools for solving Boundary Value Problems (BVP). It is addressed how stress, strain, and displacement are affected by the inhomogeneity parameter, rotation speed, pressure, temperature, and Poisson ratio. The examination of the various findings indicates that changes in the temperature profile, rotation, and inhomogeneity parameter on the thermoelastic field have a substantial impact on the stress and strain in the FGM cylinder. The findings indicate that the Poisson ratio and inhomogeneity parameters have a significant impact on the stress and deformation distributions. According to the results, the above-mentioned parameters can be adapted to control the thermoelastic filed in a FGM cylinder. The present research offers significant perspectives on the development and enhancement of rotating FGM pressure vessels intended for high-temperature applications.

* Corresponding author.
*E-mail address:* abdelhakim.benslimane@univ-bejaia.dz (A. Benslimane).

https://doi.org/10.1016/j.heliyon.2024.e31833
Received 11 August 2023; Received in revised form 16 April 2024; Accepted 22 May 2024
Available online 23 May 2024

## 1. Introduction

To improve the mechanical and thermal characteristics of structures, one strategy involves employing functionally graded materials (FGM). It is well known that Functionally Graded Materials are not homogeneous at the microscale, however, at macroscale their mechanical properties gradually change from one surface to the next in terms of the volume fractions of their constituent materials. Composites with two or more phases and continuously changing compositions along spatial positions are called functionally graded materials (FGMs). FGMs are expected to be extremely heat-resistant materials in high-temperature and high-temperature gradient environments, which has piqued the interest of many researchers recently. It has many positive aspects, including improved thermal properties, increased material strength properties, improved residual stress distribution, high modulus of resilience, high fracture toughness, potentially reduced stress intensity factor, increased corrosion resistance, and decreased in plane and transverse stresses. Besides, heat transfer and mechanical analysis is crucial for the practical deployment of FGMs in super-high-temperature and pressure situations [1]. The majority of FGM structures made of metals and ceramics are generally exposed to high thermo-mechanical loads [2]. Due to its low heat transfer and low thermal expansion factors, the ceramic phase offers greater temperature and rust protection. In addition, metal phase offers high strength, tenacity, and durability [3]. The FGM cylinders and thick walled cylindrical shells are commonly utilized in several industries to transport and store fluids under certain pressure and temperature conditions. Its application areas include power generation, chemical processing, petroleum production, biomedical research, military operations, aerospace engineering, and many more [4]. On another hand, rotary components like disks, cylinders, and spheres have found extensive use in mechanical applications and engineering. Examples of such systems encompass a wide array of machinery, including internal combustion engines, boat propellers, reciprocating and centrifugal compressors, gas rotors, steam turbines, and jet engines. Different kinds of thermal and mechanical loadings, as well as rotating body forces, can be taken into consideration [1]. Elastic studies of these mechanical devices under external or internal pressure could be highly significant for solid mechanics design.

The mechanical behavior and heat transport of FGMs have been the subject of much research by numerous scholars. Three-dimensional and two-dimensional rotating and non-rotating FGM designs exposed to thermal stress were solved for exponentially increasing characteristics using the boundary integral approach and the Gelerekin approximation in the finite element analysis (FEA) [5]. The boundary element method (BEM), which makes use of triple reciprocity relations, is widely used to tackle 2-D heat conduction problems [2]. Guo et al. [6,7] studied the behavior of cracked FGMs components under thermal shock. Two-dimensional anisotropic FGM Cauchy problems under convective boundary conditions have been investigated [8]. An accurate mathematical solution for the hyperbolic heat conduction in a FGM cylindrical vessel was given by Babaei et al. [9]. Zenkour [10] explains how a FG sandwich structure with traction behaves thermoplastically under Dirichlet thermal boundary conditions (B.Cs). A non-Fourier thermal transfer calculation with convective-radiative B.Cs for cylinders and spheres with moving and steady heat flux has been extensively studied [11–15]. Numerous analytical and numerical solutions are carried out for the case when the FGM concepts are exposed to distinct mechanical and material inhomogeneities [1,16–21]. Under thermomechanical loadings, the displacement and stress components of nonhomogeneous spherical vessels have been studied by Bayat et al. [22] in accordance with a power law in the material characteristics. Nonetheless, comparable research has been conducted by other researchers for axisymmetric rotational or irrotational vessels with fixed Poisson ratio, and a changing material inhomogeneities parameter [3,23–34]. Furthermore, cylinders subjected to steady and unstable asymmetric thermomechanical loads have been investigated [27,35]. In addition to elastic analysis, elastoplastic analysis of FGM designs is a subject of substantial research [36,37]. Nematollahi et al. [38] examine the stress and displacement fields of FGM and the impact of a magnetic field and thermo-mechanical loads on rotating FGM spheres. A nonlinear electro-thermo-elastic analysis of a spherical vessel made of FG piezoelectric materials was developed by Arefi et al. [39]. In addition to electro-thermo-elastic and electro-magneto-elastic studies, heat transmission for different FGM designs has been the subject of extensive investigation. Wang et al. [40] conducted a one-dimensional radiative-convective heat transfer research for the case of a sandwich structure. For FGM structures with both radially and tangentially changing material properties, Delouei et al. [41–44] provided an analytical solution for the heat conduction equation in spherical and cylindrical coordinate systems. The variation of attributes is analyzed using the power law in this case.

Besides from steady state and static analysis, the latest studies have also focused on dynamic and transient analysis. Souvik et al. [45] studied the dynamic behaviors of FGM sandwich panels used in thermal barrier coated turbine blades. The study explores the properties and behavior of pre-twisted straight and curved blades under various parametric conditions. Samarjeet Kumar et al. [46,47] investigate thermoelastic behavior of axially and bi-directional graded composite plates and doubly-curved panels which analyze material and geometric nonlinearities, temperature profiles, and energy equations. They also include numerical illustrations to test the fully coupled model under various conditions. In their study, Joshi et al. [48] investigates the elastoplastic characteristics of FGM composite panels including multidirectional porosities. To model the elastic properties, they adopt modified power-law functions, while the Tamura-Tomota-Ozawa model is utilized to describe the elastoplastic characteristics. A nonlinear flexural analysis has been performed for perforated FG composite panels subjected to heat conduction and uniform/sinusoidal pressure [49,50]. The studies utilize a geometrically nonlinear mathematical model with Green-Lagrange strain field and minimum potential energy method, considering single and multiple perforations. A nonlinear transient analysis of porous P-FGM and S-FGM sandwich plates and shell panels subjected to blast loading and temperature conditions is performed by Karakoti et al. [51].

Wu et al. [52] introduced a stochastic finite element model that established a correlation between measurement data and a structural model. In a recent study, Shi et al. [53] examined the behavior of a textured journal-thrust coupled bearing in an extreme thermo-mechanical environment. The study examined the impact of different parameters on lubrication performance and dynamic characteristics, considering factors such as eccentricity ratio and film thickness. Zhu et al. [54] introduced an innovative welding technique for creating a composite structure using $TA_2$ titanium and Q235 carbon steel, which are often employed in gas

transportation. They demonstrated that the application of high heat input, which leads to the formation of intermetallic compounds, causes failure at the welding contact. A new and improved technique for figuring out residual stress in welding was developed by Zhu et al. [55]. Yang et al. [56] analyzed numerically (FEA) the relationship between the structural features at different scales and the mechanical properties of Caprinae horn sheaths. The study suggested that the presence of corrugated lamellae structure might enhance fracture deflection and provide greater benefits for dry samples subjected to flexural stress. In their study, Wang et al. [57] examined the dynamic behaviors of a rotating riserless drill string by altering the rotation rate and current speed. They demonstrated that the vibrational energy of the revolving drill string is mostly focused on the rotational frequency. Fu et al. [58] examined the hydrogen embrittlement (HE) characteristics in several areas of stainless-steel joints, including the base metal, heat-affected zone, and weld metal where they analyzed the microstructures, crack propagation paths, and fracture surface appearances. Yu et al. [59] provided a novel method for producing bio-inspired composites that mimic the organic-inorganic mix and multiple-cracking fracture behavior. They successfully constructed A. pernyi composites, overcoming restrictions associated with costly raw ingredients and intricate processes. Furthermore, Li-min Tian et al. [60] investigated the collapse resistance of steel frames. Their study revealed enhancements achieved through the implementation of innovative connections, which utilize corrugated steel plates welded between the inner flange of I-shaped beams and the column.

Both disparities in the Poisson ratio and the rotation have a considerable impact on the distributions of the stress and displacement fields of thick vessels. To minimize difficulties, the Poisson ratio is, nevertheless, considered to be constant in most of the above described scenarios. To solve the problem a few number of analytical and numerical works have been conducted. A brand-new approach known as the complementary function methodology was created by Tutuncu et al. [16] to solve mechanically loaded cylinders, disks, and spheres with different stiffness and Poisson ratios. The authors in Ref. [33] constructed a finite difference model (FDM) to tackle the challenge posed by the non-uniform rotational thermoplastic behavior observed in a stacked nonhomogeneous cylinder. The cylinder was considered under to temperature-dependent data with a variable poison ratio. The non-uniform rotating thermoplastic behavior of a stacked FGM cylinder subject to temperature-dependent data with a variable poison ratio has been addressed using the finite difference technique (FDM). Additionally, research has been done on how the Poisson ratio and the inhomogeneity property of the material affect the FGM cylinder's thermo-elastic or elastic behavior [61–63]. Using the Mori-Tanaka approach, Xin et al. [64] recently investigated a FGM thick wall tube subjected to thermos-mechanical loading. Explicit forms of stress components and approximate analytical conclusions of displacement were derived by the authors. The analytical findings that were generated and those acquired using the numerical method are in good agreement. Further, the results are valid for materials with different Poisson's ratios rather than constant Poisson's ratios usually used in the existing references.

Furthermore, the power law or exponential distribution of materials in the thickness direction of the plates is used in most studies on FG plates. Using the first-order shear deformation plate theory (FSDT), Reddy and Chin [65] carried out a computational study to examine the thermomechanical behaviors of FG cylinders and plates under high heat loading conditions. They examined in their study how thermomechanical coupling affected the way FGMs responded to thermal shock. For the strain analysis, they created their own finite element code and estimated all material parameters using the linear rule of mixture. The beams with optimization demonstrated a significant increase in stiffness compared to the beams with uniformly dispersed materials, however their technique could not be applied to other objective functions. Subsequently, Najibi and Talebitooti [66] determined the thermoelastic response of 2-D FG thick cylinders by performing a nonlinear temporal heat conduction study due to temperature sensitivity of the characteristics. In order to derive thermal and consequently structural responses, the graded FEM is used to overcome the power law gradation in the 2-D FG cylinder.

Conventional FGBs (or 1D-FGBs) designed by varying material characteristics just in one direction sometimes may not meet necessary requirements, such as the temperature, hygrothermal and stress distributions in two or three directions for specific advanced construction such aircraft vehicles and shuttles. Researchers [67] have recently concentrated their efforts on an original kind of FGB with material properties that vary in two or three dimensions in order to solve this problem of the classic FGBs. Therefore, in order to generate stronger, greatly strengthened, and high-temperature resistant materials, multi-dimensional FGMs are required, through which the material characteristics are adjusted in various directions.

Based on the comprehensive literature research, it is apparent that there exists a significant level of scholarly attention towards the subject of FGM pressure vessels operating in thermo-mechanical environments. However, stresses and temperature distribution analysis in aforementioned system under generalized material characteristics still proven research gap. Moreover, in earlier studies, when the thermomechanical characteristics of the material change as a power law or exponential function of the radial position, there are analytical solutions for the elastic field in cylindrical or spherical vessels. Moreover, certain particular physical problems, such as exterior or interior boundaries where $r \to \infty$ or $r \to 0$, respectively, cannot be solved using the variation of characteristics as a power-law function. A broader method for the spatial change of stiffness, as suggested by literature, can be applied to these kinds of physical issues. Compared to previous relations, this expression offers greater freedom in modeling the shape of the stiffness profiles since it includes four configurable factors.

In addition, the effect of variable Poison ratio in stresses and displacement fields is not well developed or understood. Furthermore, there is little work in the literature that addresses the Poisson ratio and other types of material inhomogeneity in the general formula that combines the power law and exponential law. In this paper, a numerical solution is presented for the displacement and stress distributions of a rotating thick-walled cylinder made of FGM subjected to thermomechanical loading within the framework of three-dimensional elasticity theory, with a focus on the impact of the Poisson ratio and materials index parameter on the stresses and displacement fields under the various possible boundary conditions (in earlier studies which was not elaborately discussed). It was assumed that the Poisson's ratio was constant, and the material properties are given in a nonlinear general form with four parameters. The gradient variation of the elasticity module proposed in the literature was taken into consideration using a general formulation. The

equilibrium equation yields a nonlinear differential equation of second order. A model based on finite elements (FEM) was created and implemented in a FE code for a rotating tubular container subjected to thermomechanical loads. The elastic modulus was taken into consideration to gradually vary function to radial direction throughout the thickness. In the form of dimensionless graphs along the radial direction, displacement, temperature, and stress fields are shown and analyzed. It is addressed how stress, strain, and displacement fields are impacted by the inhomogeneity parameter, rotation speed, pressure, temperature, and Poisson ratio. Upon analyzing the various outcomes, it is evident that variations in temperature profile, rotation, and inhomogeneity parameter on the thermoelastic field have a considerable impact on stress and strain in the FGM cylinder. Therefore, the findings show that the aforementioned factors can be regulated in order to manage the thermoelastic filed in a FGM cylinder.

## 2. Problem formulation

In the present work, a thick rotating FGM hollow cylindrical shell with, respectively, inner and outer radius $a$, $b$ is considered subjected to thermal and mechanical loadings. The inner and outer region of the thick walled hollow cylindrical vessel are subjected at the same time, to pressure, respectively, $P_{in}$ and $P_{out}$ and temperature, respectively, $T_{in}$ and $T_{out}$.

The cylindrical vessel is made of a material which is assumed linearly elastic and isotropic and the material properties vary in space along the radial direction according to a generalized non-linear relationship. The schematization of this cylinder is shown in Fig. 1. In order to solve the problem considered under the axisymmetric hypothesis imposes the use of cylindrical coordinates system (r, θ, z). The length of the cylinder is considered sufficiently large so that we focus our attention on the plain strain problem.

It is assumed that the following generalized law (Eq. 1a, b, c, d and e) governs the variation of the Young modulus $E(r)$, thermal expansion coefficient $\alpha(r)$, thermal conductivity $k(r)$, density $\rho(r)$ and Poisson ratio $\nu(r)$ in an elastic axisymmetric plain strain problem [1]:

$$E(r) = E_{in}\left(\frac{r}{a}\right)^m \exp\left\{\gamma\left(\left(\frac{r}{a}\right)^s - 1\right)\right\}, k(r) = k_{in}\left(\frac{r}{a}\right)^m \exp\left\{\gamma\left(\left(\frac{r}{a}\right)^s - 1\right)\right\}$$
$$\alpha(r) = \alpha_{in}\left(\frac{r}{a}\right)^m \exp\left\{\gamma\left(\left(\frac{r}{a}\right)^s - 1\right)\right\}, \rho(r) = \rho_{in}\left(\frac{r}{a}\right)^m \exp\left\{\gamma\left(\left(\frac{r}{a}\right)^s - 1\right)\right\} \quad \text{(1a, b, c, d, e)}$$
$$\nu(r) = \nu_{in}\left(\frac{r}{a}\right)^m \exp\left\{\gamma\left(\left(\frac{r}{a}\right)^s - 1\right)\right\}$$

Where $m$, $\gamma$ and $s$ are real constants and $E_{in}$, $\alpha_{in}$, $k_{in}$, $\rho_{in}$ and $\nu_{in}$ are the Young modulus, thermal expansion coefficient, thermal conductivity, density and Poisson ratio at the inner surface of the cylinder ($r = a$). As a result of its four modifiable parameters, this expression offers greater modeling freedom than other relations for the shape of the material properties profiles. Power-law and exponential law profile can be obtained when considering $s = 0$ and $m = 0$, respectively, while the homogenous case is obtained when $m = 0$ and $s = 0$.

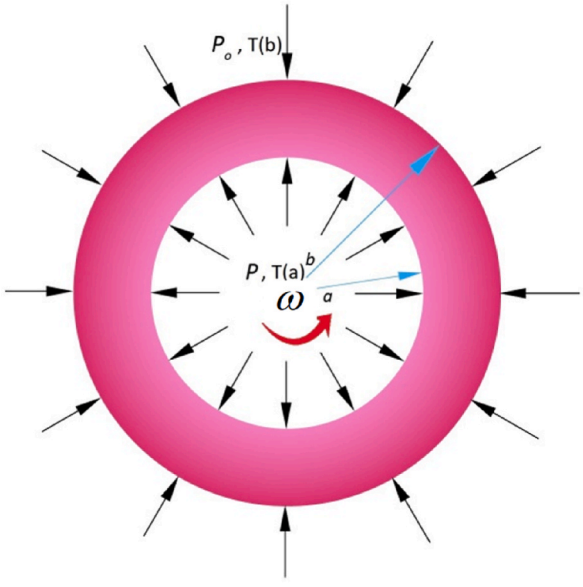


**Fig. 1.** The schematic bi-dimensional view of the rotating thick-walled cylindrical vessel subjected to thermo-mechanical load.

### 2.1. Steady state heat conduction equation

The following formula is a general steady state heat conduction equation Eq. (2) [63]:

$$\frac{1}{r}\frac{\partial}{\partial r}\left(rk(r)\frac{\partial T(r)}{\partial r}\right)+\frac{1}{r^2}\frac{\partial}{\partial \theta}\left(k(r)\frac{\partial T(r)}{\partial \theta}\right)+Q_{gen}=0 \tag{2}$$

Eq. (2) can be expressed by its form in Eq. (3) in the absence of heat generation and axisymmetric Boundary Condition (B.C.) [64]:

$$\frac{1}{r}\frac{d}{dr}\left(rk(r)\frac{dT(r)}{dr}\right)=0 \tag{3}$$

Equation (4) provides the solution to the differential equation above, which may be derived by substituting Eq. (1b) into Eq. (3):

$$T(r)=\int\left[\frac{C_1}{\varphi(r)}\right]dr+C_2$$

$$\varphi(r)=\left(\frac{r}{b}\right)^{n+1}e^{\gamma\left\{\left(\frac{r}{b}\right)^{s}-1\right\}} \tag{4}$$

#### 2.1.1. General linear B.C: (convection)

The inner and outer surfaces of a FG cylinder can be expressed as a general linear B.C. as indicated by Eq. (5):

$$A_1T(a)+B_1\frac{dT(a)}{dr}=f_1, A_2T(b)+B_2\frac{dT(b)}{dr}=f_2 \tag{5 a, b}$$

Where $A_{i=1,2}, B_{i=1,2}$ are well-known thermal parameters associated with convection and conduction coefficient, respectively. $f_{i=1,2}$ also a well-known parameter at inner and outer radii.

$C_1$ and $C_2$ are the integration constants which can be determined from Eq. (4) and Eq. (5 a, b) and are given in Eq. (6a, b) as follows:

$$C_1=\frac{\left(\int\frac{1}{\varphi(r)}\,dr\right)\Big|_{r=b}A_2f_1+\frac{1}{\varphi(b)}B_2f_1-\left(\int\frac{1}{\varphi(r)}\,dr\right)\Big|_{r=a}A_1f_2-\frac{1}{\varphi(a)}B_1f_2}{\left(\int\frac{1}{\varphi(r)}\,dr\right)\Big|_{r=b}A_2A_1+\frac{1}{\varphi(b)}B_2A_1-\left(\int\frac{1}{\varphi(r)}\,dr\right)\Big|_{r=a}A_1A_2-\frac{1}{\varphi(a)}A_2B_1}$$

$$C_2=\frac{A_1f_2-A_2f_1}{\left(\int\frac{1}{\varphi(r)}\,dr\right)\Big|_{r=b}A_2A_1+\frac{1}{\varphi(b)}B_2A_1-\left(\int\frac{1}{\varphi(r)}\,dr\right)\Big|_{r=a}A_1A_2-\frac{1}{\varphi(a)}A_2B_1} \tag{6a, b}$$

### 2.2. Analysis of mechanical and thermal stresses

In order to solve the problem considered under the axisymmetric hypothesis imposes the use of cylindrical coordinates system (r, θ, z). The displacement vector is considered by the vector $\boldsymbol{u}=(u_r \quad u_\theta \quad u_z)$, where $u_r$, $u_\theta$ and $u_z$ are the radial, circumferential and axial components of displacement vector, respectively. It is assumed that the cylinder length to be long enough to allow us to concentrate on the plain strain problem. The displacement, stress, and strain fields in the case of plane elasticity can be expressed using Eq. (7) [1]:

$$\boldsymbol{u}=\boldsymbol{u}(r), \sigma_{ij}=\sigma_{ij}(r), \varepsilon_{ij}=\varepsilon_{ij}(r) \tag{7a,b,c}$$

Where $\sigma_{ij}$ is the Cauchy stress tensor, and $\varepsilon_{ij}$ the deformation tensor. The assumption of the infinitely long cylinder and the while the elastic field is axisymmetric, the kinematic relations (strain-displacement) are given Eq. (8) [1]:

$$\varepsilon_r=\frac{du_r}{dr}, \varepsilon_\theta=\frac{u_r}{r}, \varepsilon_z=\varepsilon_{rz}=\varepsilon_{r\theta}=\varepsilon_{\theta z}=0 \tag{8a,b,c}$$

Eq. (9) expresses the relationship between stress and strain that results from the kinematics correlation in Eq. (8a, b, c):

$$\begin{Bmatrix}\sigma_r\\ \sigma_\theta\end{Bmatrix}=\begin{bmatrix}A(r) & B(r) & -C(r)\\ B(r) & A(r) & -C(r)\end{bmatrix}\begin{Bmatrix}\frac{du_r}{dr}\\ \frac{u_r}{r}\\ T(r)\end{Bmatrix} \tag{9 a, b, c}$$

$$\sigma_z=\nu(r)(\sigma_r+\sigma_\theta)-E(r)\alpha(r)T(r)$$

Where:

$$A(r)=\frac{E(r)\,[1-\nu(r)]}{[1+\nu(r)]\,[1-2\nu(r)]}\quad;\quad B(r)=\frac{E(r)\nu(r)}{[1+\nu(r)]\,[1-2\nu(r)]}\quad;\quad C(r)=\frac{E(r)\alpha(r)}{[1-2\nu(r)]}$$

$\sigma_r$, $\sigma_\theta$ and $\sigma_z$ are the radial, circumferential and axial components of the Cauchy stress tensor

By analyzing stress tensor for a cylindrical vessel in an axisymmetric problem with the presence of body force equilibrium motion equation can be derived as follows in Eq. (10):

$$\frac{d\sigma_r}{dr}+\frac{\sigma_r-\sigma_\theta}{r}+\rho(r)\omega^2 r=0 \tag{10}$$

Where $\omega$ is the rotational velocity of the cylinder. A second order governing differential equation in terms of displacement and temperature fields is produced by replacing the expression from Eq. (9a, b) in Eq. (10) as is demonstrated below in Eq. (11):

$$\frac{d^2u_r}{dr^2}+\left(\frac{1}{A(r)}\frac{dA(r)}{dr}+\frac{1}{r}\right)\frac{du_r}{dr}+\frac{1}{r}\left(\frac{1}{A(r)}\frac{dB(r)}{dr}-\frac{1}{r}\right)u_r=\frac{C(r)}{A(r)}\frac{dT(r)}{dr}+\frac{1}{A(r)}\frac{dC(r)}{dr}T(r)-\frac{\rho(r)\omega^2 r}{A(r)} \tag{11}$$

Combining Eqs. (1) and (9) with Eq. (11) yields the following deferential equation (Eq. (12)) in terms of an unknown radial displacement field.

$$\frac{d^2u_r}{dr^2}+\left\{\frac{\left[\gamma\left(\frac{r}{a}\right)^s s+m\right]\left[e^{4\gamma}-\xi_1(r)^4\nu_{in}{}^4\right]}{\xi_2(r)}+\frac{1}{r}\right\}\frac{du_r}{dr}+\frac{1}{r}\left\{\frac{2\nu_{in}\left[\gamma\left(\frac{r}{a}\right)^s s+m\right]\left[\xi_3(r)-\nu_{in}{}^2\xi_4(r)\right]}{\xi_2(r)}-\frac{1}{r}\right\}u_r$$
$$=\chi_1(r)+\chi_2(r)+\chi_3(r) \tag{12}$$

Where:

$$\xi_1(r)=\left(\frac{r}{a}\right)^m e^{\gamma\left(\frac{r}{a}\right)^s},\ \xi_2(r)=r\left\{\nu_{in}{}^2 e^{2\gamma\left(\frac{r}{a}\right)^s}\left(\frac{r}{a}\right)^{2m}-e^{2\gamma}\right\}^2,\ \xi_3(r)=\xi_1(r)e^{3\gamma}$$

$$\xi_4(r)=\left(\frac{r}{a}\right)^{3m} e^{\gamma\left(3\left(\frac{r}{a}\right)^s+1\right)},\ \chi_1(r)=\frac{\xi_1(r)\alpha_{in}\left(\nu_{in}{}^2\xi_1(r)^2-1\right)C_1}{[2\nu_{in}\xi_1(r)-1]\varphi(r)}$$

$$\chi_2(r)=\frac{2\alpha_{in}\frac{d\xi_1(r)}{dr}[\nu_{in}\xi_1(r)-1]\left[\nu_{in}^2\xi_1(r)^2-1\right]\left[C_1\int\frac{dr}{\varphi(r)}+C_2\right]}{[2\nu_{in}\xi_1(r)-1]^2}$$

$$\chi_3(r)=\frac{\rho_{in}\omega^2 r\left(\nu_{in}^2\,\xi_1(r)^2-1\right)}{E_{in}}$$

The equivalent stress ($\sigma_{VM}$), known as von Mises stress can be written in terms of stress components as given by Eq. (13) [1]:

$$\sigma_{VM}=\sqrt{\frac{3}{2}\boldsymbol{\sigma}^D:\boldsymbol{\sigma}^D} \tag{13}$$

Where $\overline{\overline{\sigma^D}}$ is the deviatoric part of the stress tensor, which is written in Eq. (14):

$$\boldsymbol{\sigma}^D=\boldsymbol{\sigma}-\frac{1}{3}tr(\boldsymbol{\sigma})\cdot\boldsymbol{I} \tag{14}$$

The stress components are given by Eq. (15):

$$\begin{cases}\sigma_r^D=\frac{1}{3}(2\sigma_r-\sigma_\theta-\sigma_z)\\ \sigma_\theta^D=\frac{1}{3}(-\sigma_r+2\sigma_\theta-\sigma_z)\\ \sigma_z^D=\frac{1}{3}(-\sigma_r-\sigma_\theta+2\sigma_z)\end{cases} \tag{15}$$

Finally, the equivalent stress can be rewritten as in Eq. (16):

$$\sigma_{VM}=\sqrt{\frac{3}{2}tr(\boldsymbol{\sigma})^2-\frac{1}{2}(tr\boldsymbol{\sigma})^2} \tag{16}$$

### 2.3. Finite element analysis (FEA)

Since an analytical solution is not feasible in this case, the differential equation (12) is solved using the conventional Galerkin

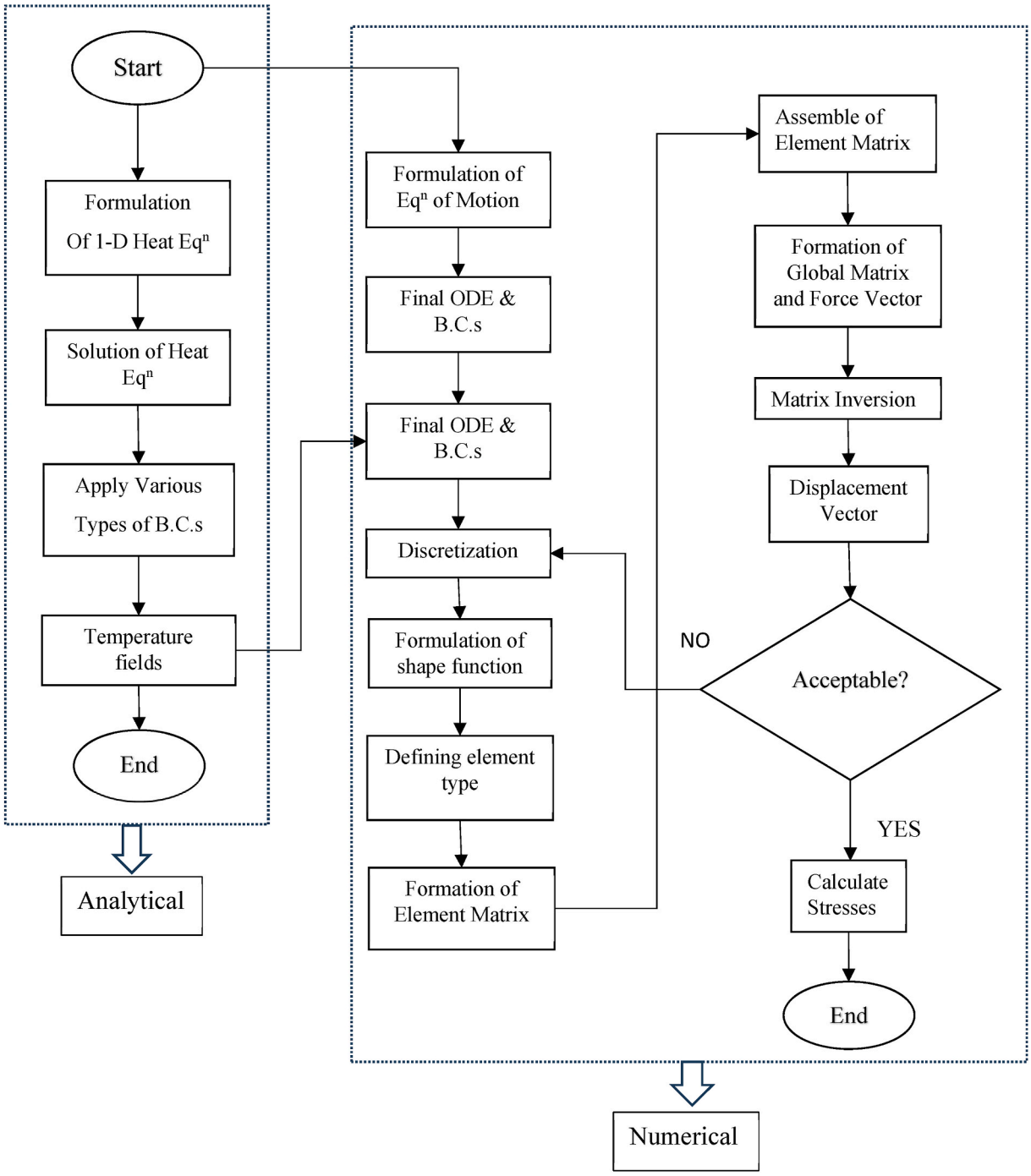


**Fig. 2.** Flow chart of finite element modeling of aforementioned problems.

discretization approach of the finite element method. The discretization process involves dividing the overall domain into N components (Eq. (17)), each of equal size, and then converting the equations into simultaneous equations.

$$\sum K_{ij} u_j{}^e = L_i{}^e \quad ; i = 1, 2 \quad e = 1, 2, \ldots\ldots N \tag{17}$$

Where the value of $K_{ij}$ and $L_i{}^e$ obtained from Eqs. (18) and (19):

$$\begin{aligned} K_{ij} \quad &= \int_{r_e}^{r_{e+1}} \frac{d\Omega_i{}^e}{d\bar{r}} \frac{d\Omega_j{}^e}{d\bar{r}} dr + \int_{r_e}^{r_{e+1}} \left\{ \frac{\left[\gamma \left(\frac{r}{a}\right)^s s + m\right] \left[e^{4\gamma} - \xi_1(r)^4 \nu_o{}^4\right]}{\xi_2(r)} + \frac{1}{r} \right\} \Omega_i{}^e \frac{d\Omega_j{}^e}{dr} dr \\ &+ \int_{r_e}^{r_{e+1}} \frac{1}{r} \left\{ \frac{2\nu_o \left[\gamma \left(\frac{r}{a}\right)^s s + m\right] [\xi_3(r) - \nu^2 \xi_4(r)]}{\xi_2(r)} - \frac{1}{r} \right\} \Omega_i{}^e \Omega_j{}^e dr + \left[\Omega_i{}^e \frac{d\Omega_j{}^e}{dr}\right]_{r_e}^{r_{e+1}} \end{aligned} \tag{18}$$

and:

$$L_i{}^e = \int_{r_e}^{r_{e+1}} \Omega_i{}^e [\chi_1(r) + \chi_2(r) + \chi_3(r)] dr \tag{19}$$

where $\Omega_i{}^e$ is linear interpolation/weighting function which can be given by following equations

$$\Omega_1^e = \frac{r_{e+1} - r}{r_{e+1} - r_e}, \Omega_2^e = \frac{r - r_e}{r_{e+1} - r_e}$$

The total domain has been modeled with 1-D two nodded linear element as mentioned above in interpolation function. Eq. (13) gives $u_j{}^e$ values at different cylinder's nodal points, which are used to determine by Eq. (20):

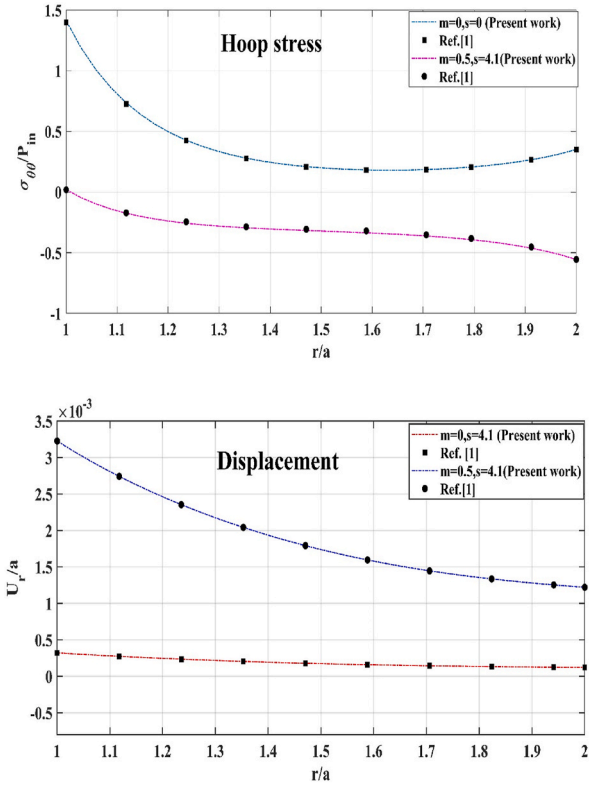


**Fig. 3.** Verification of the dimensionless hoop stress and radial displacement distributions: comparison between the obtained results and those given by Ref. [1].

$$\begin{Bmatrix}\sigma_r\\ \sigma_\theta\end{Bmatrix}=\begin{bmatrix}A(r) & B(r) & -C(r)\\ B(r) & A(r) & -C(r)\end{bmatrix}\begin{Bmatrix}\sum_{j=1}^{2} u_j{}^e\dfrac{d\Omega_j{}^e}{dr}\\ \sum_{j=1}^{2}\dfrac{u_j{}^e\Omega_j{}^e}{r}\\ T(r)\end{Bmatrix} \tag{20}$$

$$\sigma_z=\nu(r)(\sigma_r+\sigma_\theta)-E(r)\alpha(r)T(r)$$

The flow chart in Fig. 2 has been shown semi-analytical modeling of the problems where heat equation is solved using analytical method but equation of motion carried out numerically (FEM).

A number of variables affect the computational resources (time and memory) required to solve the steady-state issue for a cylindrical body using the suggested approach. These variables include the problem's dimensions, sometimes known as the mesh size, the numerical solver selected, the particular characteristics of the material, and the boundary conditions included. The recommended method efficiently reduces the mathematical intricacy and enhances the grid size. Consequently, when compared to other techniques like FDM, FVM, and DQM, the memory and time needs are greatly lowered. In summary, the proposed method performs well in terms of computation time, memory usage, scalability, accuracy and precision, resilience, ease of use and implementation, parallelization, and resource needs.

## 3. Results and discussions

### 3.1. Validation and mesh independency test

Outcomes of dimensionless radial displacement and hoop stress distributions for functionally graded cylindrical vessel are shown in Fig. 3 in order to assess the validity and accuracy of the used numerical solution. Comparisons are made between the outcomes of the current numerical formulation and those from Ref. [1]. The obtained numerical results are in excellent agreement with the results obtained by Ref. [1].

However, the optimized element estimated approximately 1000 which shown in grid independency test in Fig. 4.

### 3.2. Current results

In the present section, a thick-walled cylinder made of a functionally graded material is considered to illustrate the effectiveness of the obtained finite element solution. The inner and outer radii are $a = 1$ m and $b = 2$ m (b = 2a), respectively. The numerical values of thermo-mechanical properties at the inner region of the cylinder considered in the present work are summarized in Table 1.

The cylinder studied is subject to different thermo-mechanical boundary conditions in order to study the stress, temperature and displacement fields under different service conditions. Thus, the pressures that operate on the inside and outside surfaces of the cylinder are $P_{in} = 50$ MPa, $P_{out} = 0, 50$ MPa, respectively while the angular velocity is taken $\omega = 260, 300, 340, 380$ and 420 rad/s. The applied temperature at internal and external surfaces are $T_{in} = 700$ K, $T_{out} = 400$ K, respectively.

In order to create a specific condition for analysis, the constant values in Eq. (1) are fixed $\gamma = 0.172$ and $s = 4.1$ according to Benslimane et al. [1]. However, the constants can be chosen in different ways to reproduce different spatial variations shapes of the properties across the cylinder thickness. The investigation was then performed on the effect of the variation of the non-homogeneity parameter $m = -5$, $-4$ and $-3$ on the stress, temperature and displacement fields.

The evolution of dimensionless material properties along a radial direction is depicted in Fig. 5, with various values of $m = -5$, $-4$ and $-3$, corresponding to different ratios of the material properties $\{E(r)/E_{in}, \rho(r)/\rho_{in}, \alpha(r)/\alpha_{in}, \nu(r)/\nu_{in}, k(r)/k_{in}\} \equiv 0.5, 1$ and 2, respectively. Fig. 5 makes it clear that for a certain radius $r$ ($r \in [a, b]$), each dimensionless characteristic value grows as the non-

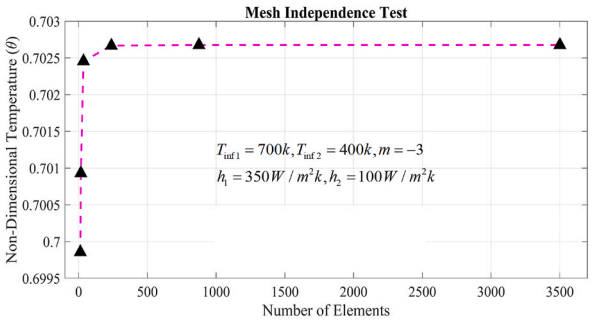


**Fig. 4.** Grid independence test.

**Table 1**
The thermo-mechanical characteristics at the inner region of the cylindrical vessel.

| Material propriety | Symbol | Value | Unit |
|---|---|---|---|
| **Young Modulus** | $E_{in}$ | 200 | GPa |
| **Thermal expansion** | $\alpha_{in}$ | $1.2 \times 10^{-6}$ | $1/k$ |
| **Thermal conductivity** | $k_{in}$ | 35 | $Wm^{-1}k^{-1}$ |
| **Density** | $\rho_{in}$ | 1500 | $Kgm^{-3}$ |
| **Poisson ratio** | $\nu_{in}$ | 0.23 | – |

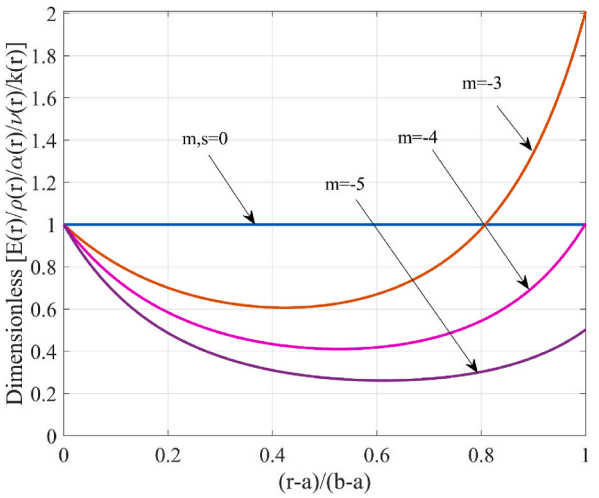


**Fig. 5.** The variation of dimensionless material properties along the radial direction with various values of $m$.

homogeneity parameter $m$ rises. It is important to notice that the graphic also shows the homogeneous scenario ($m = 0$ and $s = 0$), in which every material property is constant and represented by a horizontally straight line.

**CASE I.** Cylinder subjected to thermal Dirichlet boundary conditions with pressure loading

The non-homogeneous cylinder considered in this first case is subject to thermo-mechanical boundary conditions that can be summarized as follows: Internal and external pressure, respectively, $P_{in} = 50$ MPa, $P_{out} = 0$ MPa are applied to the inner and outer surfaces of the cylinder. The inner and outer surfaces of the cylinder are also subjected to internal and external temperatures, respectively, $T_{in} = 700$ K, $T_{out} = 400$ K.

Under the prescribed thermo-mechanical boundary condition, the effect of material inhomogeneity $m$ on the temperature, displacement and stress fields was studied.

The evolution of the dimensionless temperature ($\theta = T(r)/T_{in}$) along the radial direction through the cylinder thickness is illus-

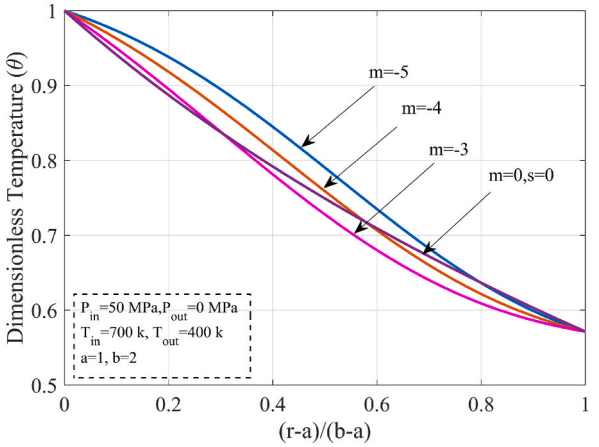


**Fig. 6.** Temperature evolution through the radial direction of the cylinder under thermal Dirichlet boundary conditions with pressure loading.

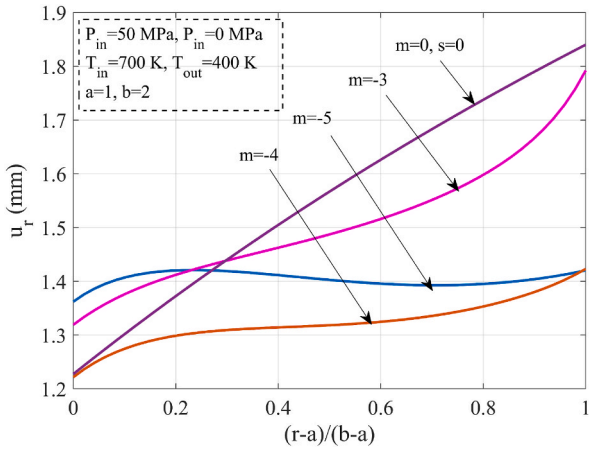


**Fig. 7.** Displacement field through the radial direction of the cylinder under thermal Dirichlet boundary conditions with pressure loading.

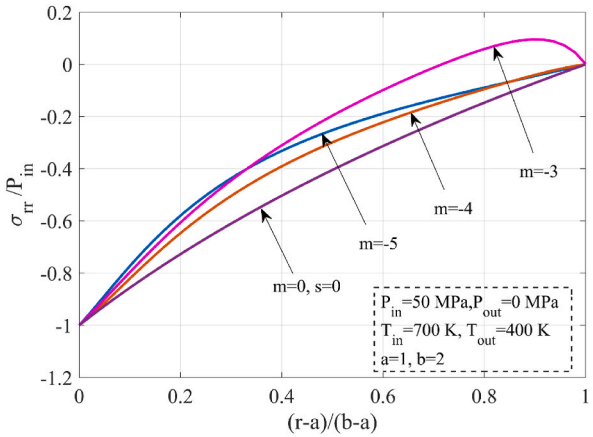


**Fig. 8.** Dimensionless radial stress component through the radial direction of the cylinder under thermal Dirichlet boundary conditions with pressure loading.

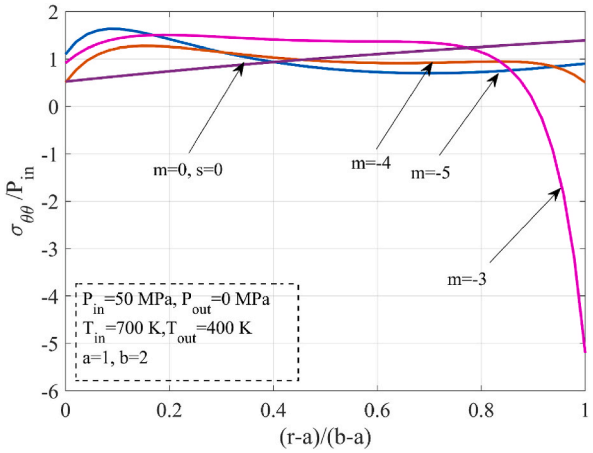


**Fig. 9.** Dimensionless circumferential stress component through the radial direction of the cylinder under thermal Dirichlet boundary conditions with pressure loading.

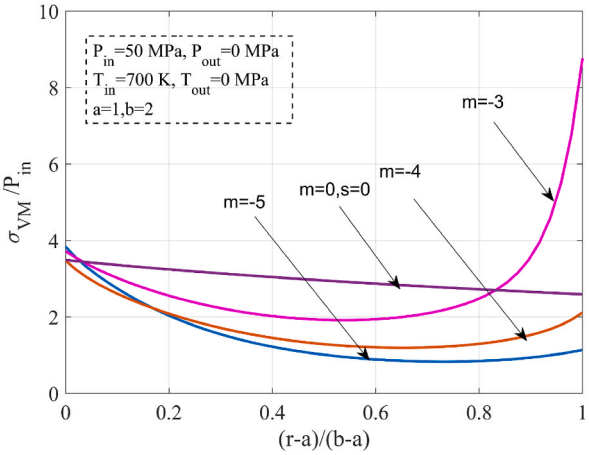


**Fig. 10.** Dimensionless equivalent stress through the radial direction of the cylinder under thermal Dirichlet boundary conditions with pressure loading.

trated for different values of the non-homogeneity parameter $m$ in Fig. 6. For all values of $m$, the dimensionless temperature exhibits its maximum values on the inner surface of the cylinder and then monotonically decreases across the cylinder's width to attain its lowest levels on the exterior of the cylinder. The graph makes it clear that, for a given radius $r$ ($r \in [a,b]$), the temperature is inversely proportional to the non-homogeneity parameter $m$, meaning that as m decreases, the temperature rises.

By taking into account various non-homogeneity parameter ($m = -5$, $-4$ and $-3$) values in Figs. 7–10 is plotted the distribution of, respectively, the radial displacement ($u_r$), radial ($\sigma_{rr}/P_{in}$), circumferential ($\sigma_{\theta\theta}/P_{in}$) and equivalent ($\sigma_{VM}/P_{in}$) stresses resulted from the numerical solution across the thickness under coupled internal pressure and temperature loading.

Fig. 7 illustrates the evolution of radial displacement along the radial direction under prescribed boundary condition and for different values of non-homogeneity, parameter $m$. Fig. 7 clearly shows that the internal surface ($r = a$) is where the radial displacements present their lowest values. It is interesting to note that for lower values of non-homogeneity parameter $m$ ($m = -5$ and $-4$) the displacement shows an increasing evolution from the inner surface followed by a plateau and then a slight increase near the outer surface. This is because local thermal stress predominates over mechanical stress (as it subjected to high thermal load), and since inhomogeneity parameter properties are strong at the inner and outer surfaces, it causes displacements that are increasing nature at the inner and outer surfaces. In this case, increasing values of $m$ leads to an increase in the magnitude values of displacement.

However, by increasing the value of non-homogeneity parameter $m$ ($m = -3$ and 0), especially for the homogeneous case ($m$, $s = 0$), the displacement shows a monotonically increasing evolution along the radial direction. Increasing values of $m$ in the inner region of the cylinder when $(r-a)/(b-a) \sim\prec 0.3$ leads to a decrease in the magnitude values of displacement while an inversed phenomenon is observed when $(r-a)/(b-a) \sim\succ 0.3$ where increasing values of $m$ leads to an increase in the magnitude values of displacement.

Moreover, this results can be explained by the fact that in the range of values of the non-homogeneity parameter ($m = -5$ and $-4$) the mechanical properties of the material are predominant as well. Indeed, the higher the Young modulus of a material, the greater its resistance to deformation and the lower the displacement it experiences for a given amount of stress. Therefore, increasing the Young modulus of a material help to reduce the amount of displacement, which can in turn reduce the stresses that develop within the material. While for higher the non-homogeneity parameter ($m = -3$ and 0) the thermal properties of the material become predominant. In fact, an increase in thermal conductivity associated with an increase in thermal expansion coefficient, can in turn lead to greater displacement. This is because a material with a higher thermal expansion coefficient will tend to undergo greater deformation or strain in response to temperature changes.

The dimensionless radial stress component ($\sigma_{rr}/P_{in}$) is plotted in Fig. 8 for different values of non-homogeneity parameter $m = -5$, $-4$ and $-3$. The homogeneous case ($m$, $s = 0$) is also shown. In terms of radial stress variation, homogeneous and heterogeneous materials are comparable. It is clear from Fig. 8 that the radial stress at the inner and outer surfaces of the nonhomogeneous cylindrical vessel satisfies the specified axisymmetrical boundary conditions. The magnitude of the radial stress exhibits a monotonic behavior rising with $r$ for all values of non-homogeneity index $m$ that were taken into consideration.

The results can be explained by the fact that, within a specific range of values of the non-homogeneity parameter (m = −5 and −4), the mechanical properties of the material are the primary factor influencing its behavior. This is because a material with a higher elastic modulus will be more resistant to deformation, resulting in lower displacement for a given stress level. Therefore, increasing the overall stiffness of the material can help to reduce displacement, leading to lower stress levels.

However, for higher values of the non-homogeneity parameter (m = −3 and 0), the thermal properties of the material become more significant. An increase in thermal conductivity, combined with an increase in thermal expansion coefficient, can lead to greater displacement. This is because a material with a higher thermal expansion coefficient will undergo greater deformation in response to temperature changes, resulting in higher stress levels.

Fig. 9 illustrates the evolution of dimensionless circumferential stress component ($\sigma_{\theta\theta}/P_{in}$) along the radial direction for several

non-homogeneity parameter $m$ ($m = -5$, $-4$ and $-3$). The homogeneous case ($m$, $s = 0$) is also plotted in the figure. Both homogeneous and heterogeneous materials exhibit similar circumferential stress evolution. It is noteworthy to note that for lower values of non-homogeneity parameter $m$ ($m = -5$ and $-4$) the circumferential stress exhibit a slight increasing nature from the inner surface followed by a plateau and then a slight decrease near the outer surface. In the inner region of the vessel $(r-a)/(b-a) \sim\prec 0.3$, increasing values of $m$ leads to a decrease in the magnitude values of circumferential stress while in the outer region increasing values of $m$ leads to a slight increase in the magnitude values of circumferential stress. However, by increasing the value of non-homogeneity parameter $m$ ($m = -3$), the circumferential stress shows a slight increasing evolution followed by a plateau along the radial direction then a strong decrease in its magnitude near the outer surface. The magnitude of the circumferential stress for $m = -3$ along almost all the thick-wall is higher than the magnitude of the circumferential stress calculated for the other lower values of the non-homogeneity parameters.

Fig. 10 illustrates the evolution of the equivalent stress known as Von-Misses stress ($\sigma_{VM}/P_{in}$) for various material non-homogeneity parameters $m$ ($m = -5$, $-4$ and $-3$) where the homogeneous case ($m$, $s = 0$) is given as reference. It is obvious to see from Fig. 10 that the equivalent stress has a decreasing increasing nature along the radial direction. For the lower values of the non-homogeneity parameters $m$ ($m = -5$ and $-4$), the equivalent stress shows a slight increase at the outer surface of the cylindrical vessel, however, it does not exceed the yield stress indicating a safety operation limit. Otherwise, the increase observed for the non-homogeneity parameter $m$ = -3 near the outer surface is exponential and far exceeds the yield stress.

- **Effect of Poisson ratio**

The effect of Poisson ratio on the displacement and stress fields is investigated by considering different cases of FGM cylinders with a variable Poisson ratio (i.e. following Eq. (1e) with different non-homogeneity parameter) which are compared to the simple case where the Poisson ratio is considered as a constant.

Fig. 11 illustrates the evolution of the displacement along the radial direction for three values of Poisson ratio taken as a constant ($\nu$ = 0.25, 0.3 and 0.35) while the other physical properties are set for a fixed non-homogeneity parameter ($m$ = -3). The curves are presented in the figure with dashed lines. It is obviously seen that the increase of the values of the Poisson's ratio generates more important radial displacement fields. The solid lines show the evolution of radial displacement for various non-homogeneity parameters.

The effect of Poisson ratio on the stress field can be seen in Figs. 12 and 13. The evolution of radial stress component for various constant of Poisson ratio (dashed lines) is compared with variable Poisson ratio (solid lines) for different values of non-homogeneity parameter in Fig. 12. It is noteworthy to mention that increasing in Poisson ratio leads to a decrease in the radial stress component.

Fig. 13 illustrates the evolution of circumferential stress component for various constant of Poisson ratio (dashed lines) which is compared with curves of variable Poisson ratio (solid lines) for different values of non-homogeneity parameter. It is noteworthy to mention that increasing in Poisson ratio leads to a decrease in the circumferential stress component.

- **Effect of internal temperature**

In order to investigate the effect of thermal stresses on the displacement and stress fields generated through the cylinder wall, different boundary conditions were used, namely: a varying internal temperature ($T_{in} = 423, 473, 523, 573$ and $700$ K) while the external applied temperature is fixed ($T_{out} = 298$ K). Fixed internal and external pressure, respectively, $P_{in} = 50$ MPa, $P_{out} = 0$ MPa are applied to the inner and outer surfaces of the cylinder. For the clarity of the figures the study was conducted on a single parameter of non-homogeneity $m$ ($m = -5$).

The evolution of displacement for a specific non-homogeneity parameter $m$ ($m = -5$) is illustrated in Fig. 14 in order to investigate

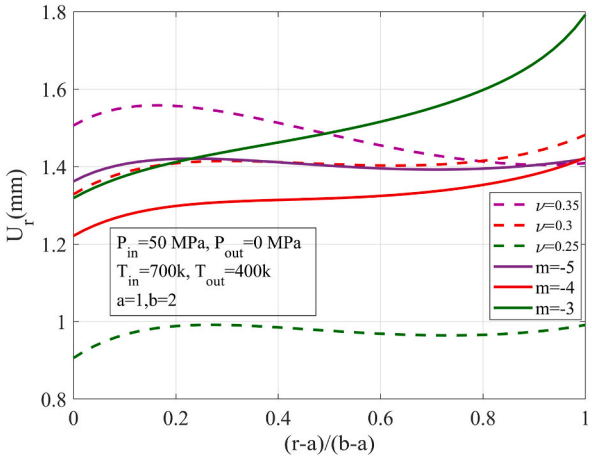


**Fig. 11.** Displacement through the radial direction of the cylinder subjected to pressure loading and various Poisson ratio.

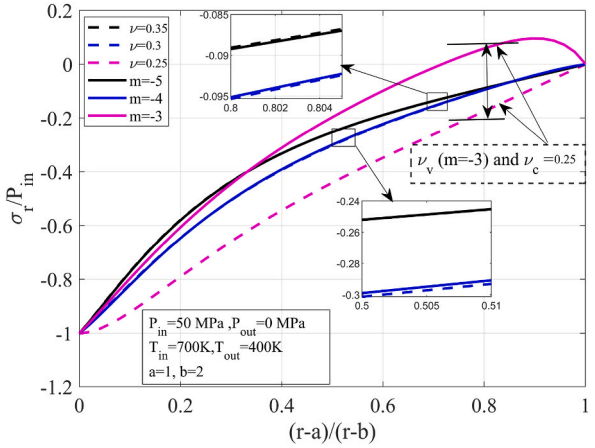


**Fig. 12.** Dimensionless radial stress component through the radial direction of the cylinder subjected to pressure loading and various Poisson ratio.

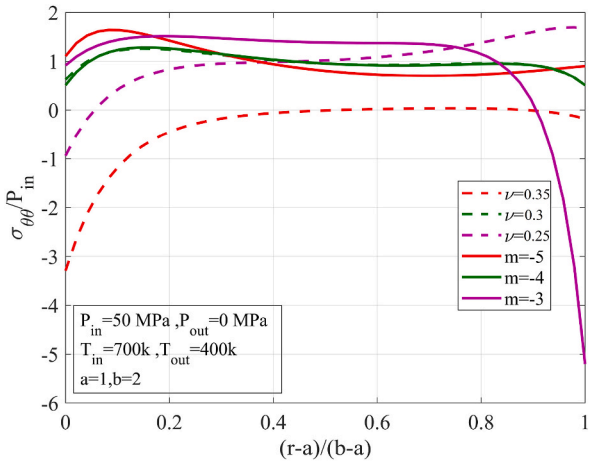


**Fig. 13.** Dimensionless circumferential stress component through the radial direction of the cylinder subjected to pressure loading and various Poisson ratio.

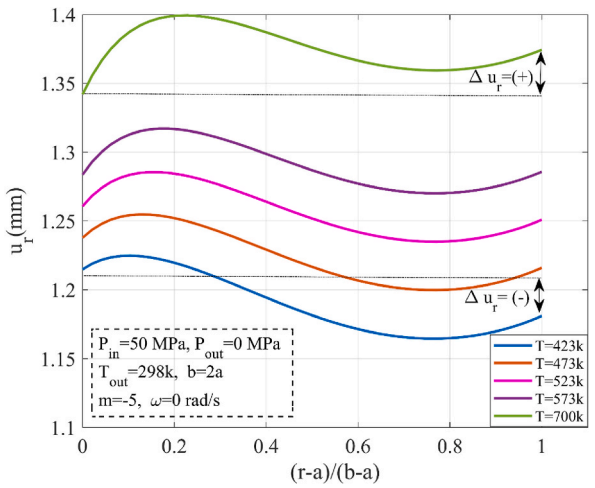


**Fig. 14.** Displacement through the radial direction of the cylinder subjected to pressure loading and various internal temperatures while the external temperature and non-homogeneity parameter are fixed.

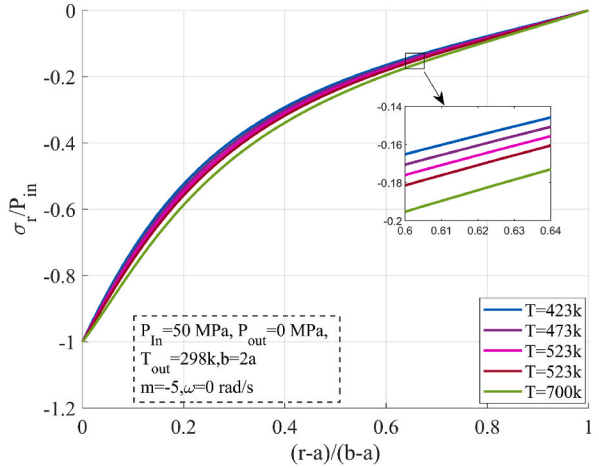


**Fig. 15.** Dimensionless radial stress through the radial direction of the cylinder subjected to pressure loading and various internal temperatures while the external temperature and non-homogeneity parameter are fixed.

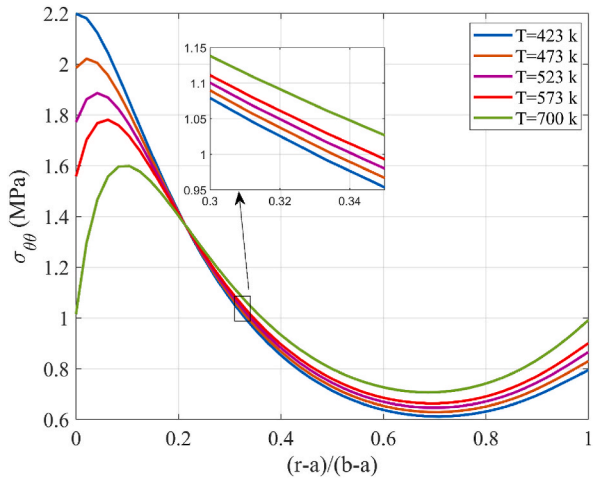


**Fig. 16.** Dimensionless circumferential stress through the radial direction of the cylinder subjected to pressure loading and various internal temperatures while the external temperature and non-homogeneity parameter are fixed.

the effect of imposed internal temperature. It is clear from the figure that the thermal gradient between the inner and outer surfaces has a significant effect on the displacement field. Indeed, by increasing the applied temperature on the internal surface of the cylinder an increase of the displacement is observed while the shape of the curves remains unchanged: a shift towards higher values occurs. In general, increasing the temperature of a material will cause it to expand and therefore increase its strain. This is because as the temperature of a material increases, the average kinetic energy of its atoms or molecules increases, causing them to move more vigorously and increase the spacing between them.

In order to investigate the effect of imposed internal temperature on the evolution of dimensionless radial stress component, Fig. 15 illustrates dimensionless radial stress curves for a fixed non-homogeneity parameter $m$ ($m = -5$) and various internal temperatures. The increases in internal temperature leads to a decrease in radial stress. In fact, increase in temperature lead to a decrease in the internal forces within the material, resulting in a decrease in stress known as thermal softening behavior which is an important consideration in the design of high-temperature applications.

Fig. 16 illustrates dimensionless circumferential stress curves for a fixed non-homogeneity parameter $m$ ($m = -5$) and various internal temperatures. From the stress curves, two regions through the cylinder thickness can be recognized: an inner region $(r-a)/(b-a) \sim\prec 0.22$ where an increase in temperature results in a decrease in stress and an outer region $(r-a)/(b-a) \sim\succ 0.22$ where an increase in temperature results in an increase in stress. It should be noted that at $(r-a)/(b-a) \approx 0.22$ curves converge.

•Effect of internal pressure

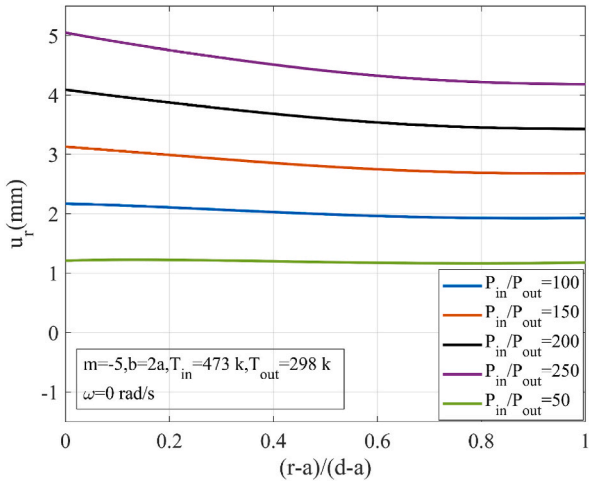


**Fig. 17.** Displacement through the radial direction of the cylinder subjected to different pressure loading. Internal temperature and non-homogeneity parameter are fixed.

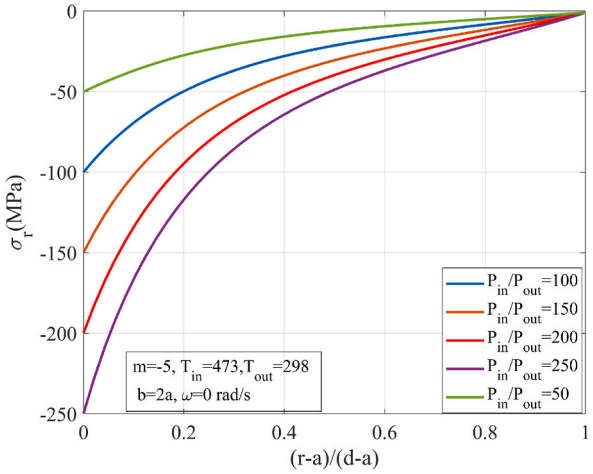


**Fig. 18.** Radial stress component through the radial direction of the cylinder subjected to different pressure loading. Internal temperature and non-homogeneity parameter are fixed.

In this part, the effect of different applied pressure gradient by varying internal pressure on the displacement and stress fields was investigated while the temperature gradient and the non-homogeneity parameter were kept fixed. Fig. 17 illustrates displacement curves when the cylinder is subjected to various internal pressures. As can be predicted, the increase in internal pressure results in an increase in displacement through the thickness of the cylinder.

The increase in internal pressure also results in an increase in radial and circumferential stress components through the thickness of the cylinder, as it can be shown in Figs. 18 and 19. The generated radial and circumferential stresses are compressive and tensile, respectively, in the radial direction.

**CASE II.** Cylinder subjected to thermal Robins type boundary conditions (Convection) with pressure loading

In the second case, a non-homogeneous cylinder is considered under thermo-mechanical boundary conditions that can be summarized as follows: The mechanical boundary conditions are considered for inner surface with traction and outer surface traction free, respectively, $P_{in} = 50$ MPa, $P_{out} = 0$ MPa coupled to an imposed rotation velocity $\omega = 300$ rad/s. The inner and outer surfaces of the cylinder are also subjected to convection type boundary conditions with internal and external temperatures, respectively, $T_{\inf 1} = 700$ K, $T_{\inf 1} = 400$ K. The film coefficients are considered at inner and outer surface, respectively, $h_1 = 350$ W/m$^2$K, $h_2 = 100$ W/m$^2$K.

Under the prescribed thermo-mechanical boundary conditions, displacement and stress fields was investigated for various material inhomogeneity $m$. By taking into account various non-homogeneity parameter ($m = -5, -4$ and $-3$) values in Figs. 20–23 is plotted the distribution of, respectively, the radial displacement $(u(r))$, radial $(\sigma_{rr}/P_{in})$, circumferential $(\sigma_{\theta\theta}/P_{in})$ and equivalent $(\sigma_{VM}/P_{in})$ dimensionless stresses resulted from the numerical solution across the thickness under coupled mechanical and thermal loadings.

Under prescribed mechanical and thermal boundary condition, radial displacement is shown in Fig. 20 for several types of FGM

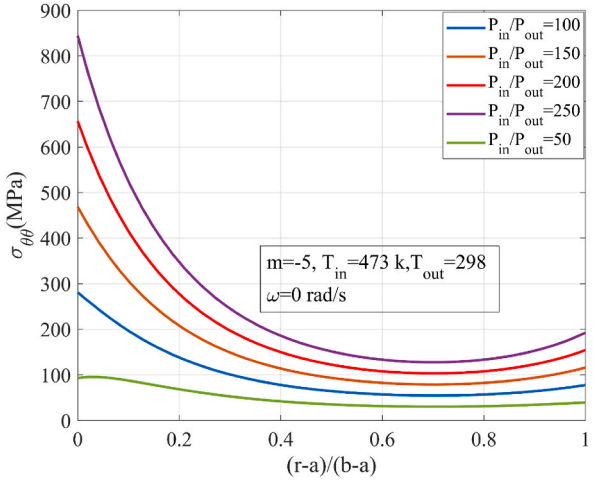


**Fig. 19.** Circumferential stress component through the radial direction of the cylinder subjected to different pressure loading. Internal temperature and non-homogeneity parameter are fixed.

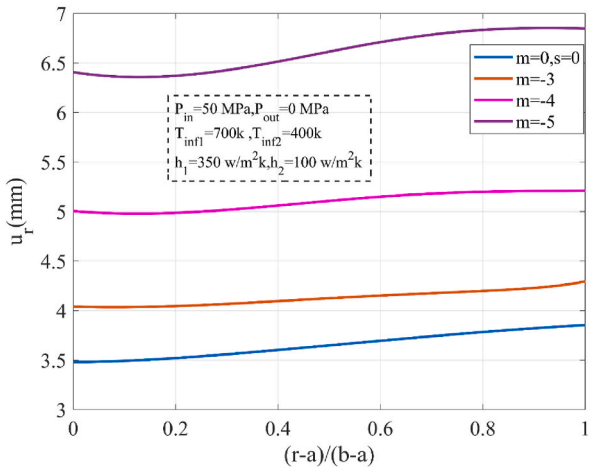


**Fig. 20.** Displacement field through the radial direction of the cylinder under thermal convection boundary conditions with pressure loading.

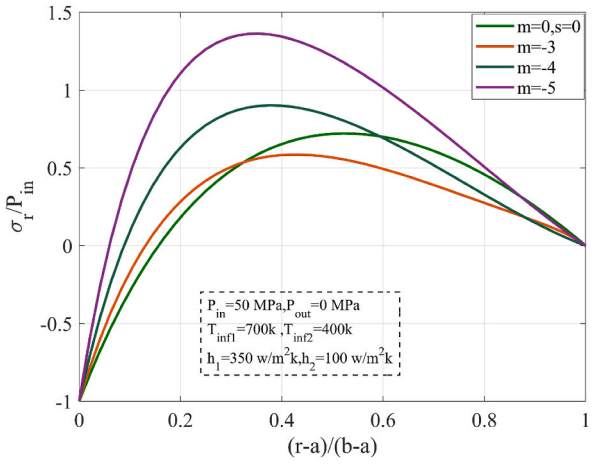


**Fig. 21.** Dimensionless radial stress through the radial direction of the cylinder under thermal convection boundary conditions with pressure loading.

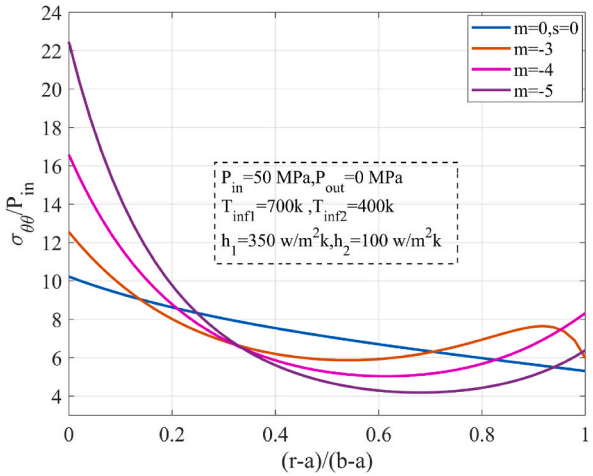


**Fig. 22.** Dimensionless circumferential stress through the radial direction of the cylinder under thermal convection boundary conditions with pressure loading.

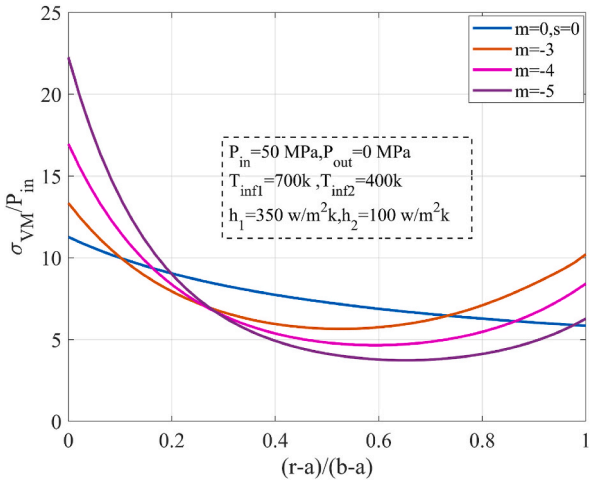


**Fig. 23.** Dimensionless equivalent stress through the radial direction of the cylinder under thermal convection boundary conditions with pressure loading.

cylinders by varying the non-homogeneity parameter $m$. The shape of the displacement curves shows an almost constant evolution along the radial direction with a slight increase towards the outer region of the cylinder. However, for a fixed radius $r$ ($r \in [a, b]$) an increase in the values of the non-homogeneity parameter results in an increase in the magnitude of the displacements. Indeed, when $m$ goes higher values, the material becomes stiffer and this leads to a quicker increase in displacement.

Fig. 21 illustrates the evolution across the thickness of the dimensionless radial stress with different non-homogeneity parameters. It can be seen that there is an increase and decrease in the dimensionless radial stress component. The inner region of the cylinder experiences compressive stress, whereas the outer region experiences tensile stress, for all non-homogeneity factors examined. The maximum and minimum tensile stresses are observed, respectively, for $m = -5$ and $m = -3$ which are located at $(r-a)/(b-a) \approx 0.3$.

Fig. 22 shows the evolution along the radial direction of the dimensionless circumferential stress for different non-homogeneity parameters. Despite the radial stress, the dimensionless circumferential stress component exhibits a reducing and growing character. Its greatest magnitude value for all non-homogeneity parameters is found on the interior surface of the cylinder. The circumferential stress component is tensile stress through the thickness of the cylinder. From the circumferential stress curves, two regions through the cylinder thickness can be recognized: an inner region $(r-a)/(b-a) \sim\prec 0.3$ where an increase in non-homogeneity parameter results in a decrease in stress and an outer region $(r-a)/(b-a) \sim\succ 0.3$ where an increase in non-homogeneity parameter results in an increase in stress. It should be noted that at $(r-a)/(b-a) \approx 0.3$ curves converge.

Fig. 23 displays how the non-homogeneity characteristic affects the variation of equivalent stress in a radially direction. The dimensionless equivalent stress component is diminishing and increasing in nature. Its highest magnitude value for all non-homogeneity parameters occurs on the inner surface of the cylinder. As seen above, for circumferential stress, the dimensionless

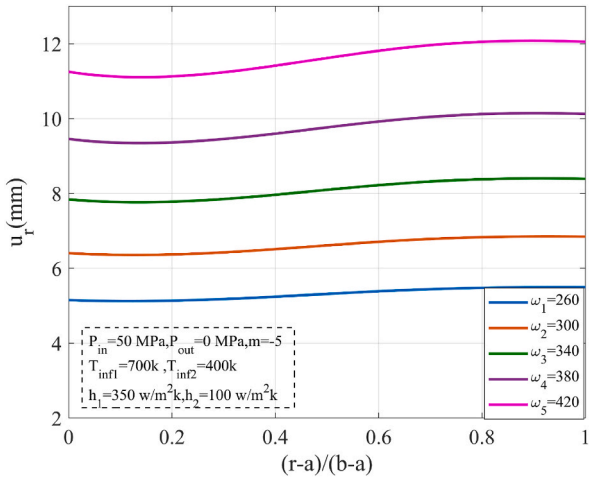


**Fig. 24.** Radial displacement through the radial direction of the cylinder under thermal convection boundary conditions with pressure loading for varying rotational speed.

value of radial position $(r-a)/(b-a) \approx 0.3$ is a convergent point for all curves. However, in inner region $(r-a)/(b-a) \sim \prec 0.3$ an increase in $m$ leads in a decrease in equivalent stress while in outer region $(r-a)/(b-a) \sim \succ 0.3$ an increase in $m$ parameter results in an increase in stress.

- **Effect of rotational speed**

In order to investigate the effect of rotation speed on the displacement and stress field, a thick-walled cylinder is considered under the thermos-mechanical loadings presented in the second case for varying rotational speed $\omega = 260, 300, 340, 380$ and 420 rad/s. For the clarity of the figures only one non-homogeneity parameter ($m = -5$) is taken into consideration.

Fig. 24 shows the radial displacement through the thickness of the cylinder under pressure gradient and thermal convection boundary conditions for various rotational speed. It is clear from the figure that the rotation speed has a considerable effect on the displacement field where the magnitude of displacement depends on the speed of rotation. As can be predicted, at higher rotation speeds, the centrifugal force generated by the vessel is greater, resulting in a more significant displacement field.

Figs. 25 and 26 illustrate clearly how the rotational speed affect the stress field. The dimensionless radial stress component for various rotational speed is shown in Fig. 25. It shows an increasing decreasing nature. Radial stress shows a compressive stress in internal region while it shows a tensile stress elsewhere. As can be seen for displacement field, at higher rotation speeds, the centrifugal force generated leads in a more significant radial stress.

Fig. 26 illustrates dimensionless circumferential stress component for various rotational speed. Circumferential stress shows a decreasing nature along the radial direction where the maximum value is observed on the inner surface of the cylinder. It is tensile

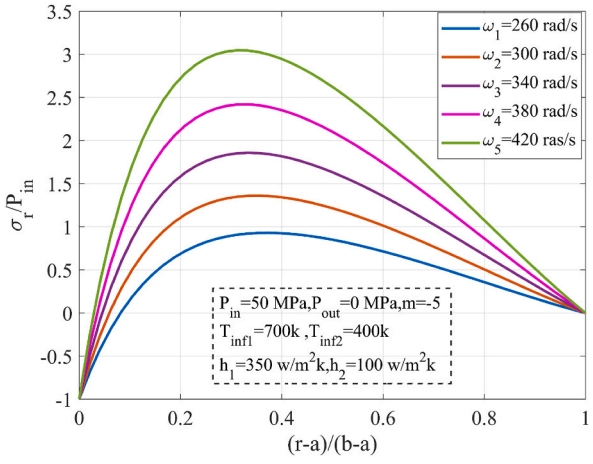


**Fig. 25.** Dimensionless radial stress through the radial direction of the cylinder under thermal convection boundary conditions with pressure loading for varying rotational speed.

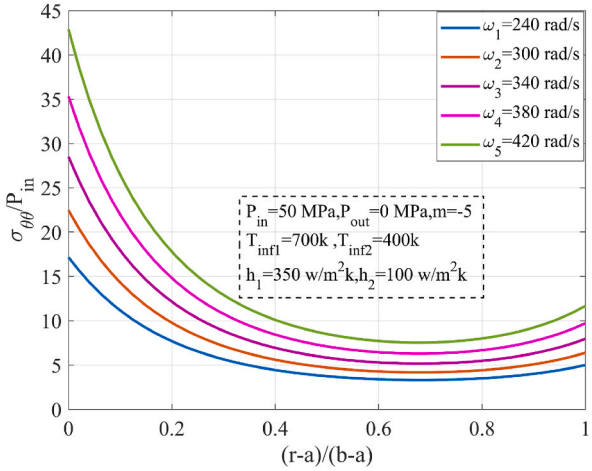


**Fig. 26.** Dimensionless circumferential stress through the radial direction of the cylinder under thermal convection boundary conditions with pressure loading for varying rotational speed.

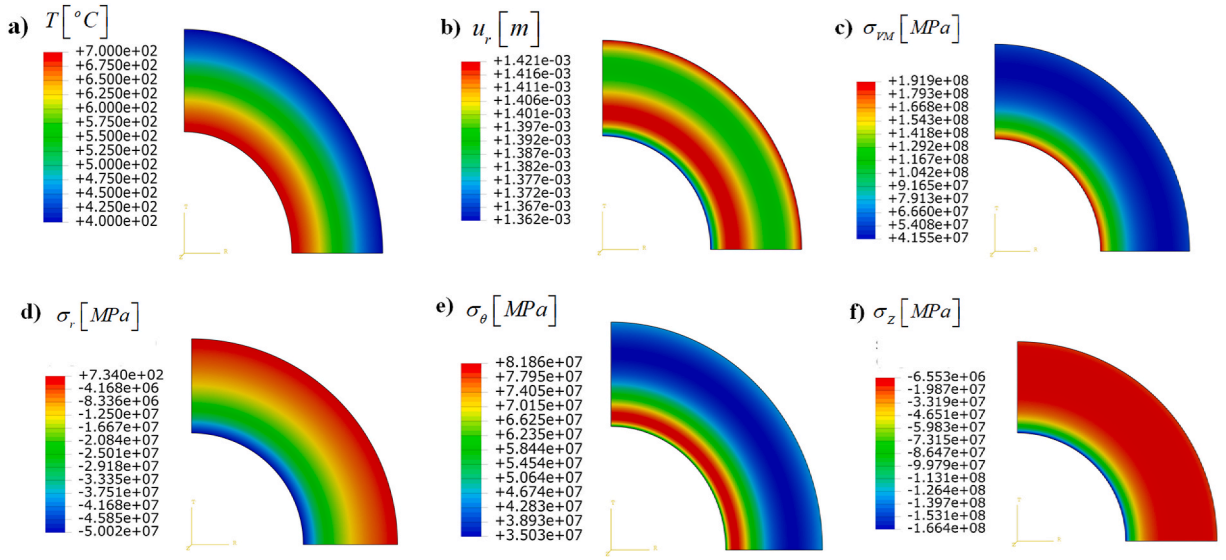


**Fig. 27.** Dimensional contour plots of several output parameters, including: a) temperature, b) radial displacement, c) Von-Misses stress, d) radial stress, e) hoop stress, and f) axial stress.

stress everywhere across the thickness. By increasing the speed of rotation, the same results obtained previously are observed, i.e. an increase in the magnitude of the circumferential stress component.

However, Fig. 27 displays dimensional contour plots of several output fields including temperature, radial displacement, Von-Misses stress, radial stress, hoop stress, and axial stress.

## 4. Conclusions

The aim of this study was to develop a numerical formulation that could be used to explore the thermo-elastic fields within a rotating thick-walled cylinder composed of non-homogeneous material under various thermal and mechanical loads. The change in the material characteristics was thought to follow a broad nonlinear expression throughout the cylinder's thickness. From the mechanical equilibrium equation, Navier's second-order ordinary differential equation is obtained. The partial differential equation is solved using a conventional Galerkin discretization technique of the finite element method, yielding a numerical solution for the displacement and stress profiles. Results show that the gradient of temperature between the inner and outer surfaces, the angular velocity, the internal and external pressure, and the spatial variation of thermal and mechanical properties all have a substantial impact on the thermoelastic field in a FGM cylinder. The main conclusions drawn are as follows.

- First, a pressurized hollow functionally graded cylindrical vessel was used to examine the influence of grading parameter. It was discovered that the strength of the hollow cylindrical vessel increased as grading parameter was increased. As a result, the radial stress component and displacement magnitude decrease. Therefore, increasing the Young modulus of a material help to reduce the amount of displacement, which can in turn reduce the stresses that develop within the material.
- The effect of Poisson ratio on the displacement and stress fields is investigated by considering different cases of FGM cylinders with a variable Poisson ratio. It is obviously seen that the increase of the values of the Poisson's ratio generates more important radial displacement fields. However, increasing in Poisson ratio leads to a decrease in the radial and circumferential stress components.
- After that, the impact of thermal loading was examined, and it was discovered that when temperature increased, so strain in increased, which caused the material stiffness to decrease. As a result, the radial stress component and displacement magnitude increase.
- Finally, research on the impact of centrifugal force revealed that radial and tangential stress components rise with increasing angular velocity.

These results suggest that the distribution of stresses and radial displacement in a cylinder composed of functionally graded material (FGM) is strongly influenced by the spatial variation of mechanical and thermal properties. The degree of heterogeneity can therefore be altered to satisfy particular needs and control the distribution of stresses, making it a crucial consideration during the design process. However, it might be beneficial for the future endeavors work to consider incorporating temperature-dependent material properties within their analysis. This addition could significantly enhance the comprehensiveness of the present study, offering a more realistic portrayal of the FG material behavior under varying thermal conditions.

## Declarations

Conflict of interest No potential conflict of interest was reported by the author(s)

## CRediT authorship contribution statement

**P. Das:** Writing – review & editing, Writing – original draft, Validation, Software, Investigation, Formal analysis, Conceptualization. **A. Benslimane:** Writing – review & editing, Writing – original draft, Methodology, Investigation. **M.A. Islam:** Methodology, Conceptualization. **A.A. Siddiquei:** Methodology, Conceptualization. **M.M. Rahman:** Methodology. **Md Mahmudul Adil:** Writing – review & editing, Validation.

## Declaration of competing interest

The authors declare that they have no known competing financial interests or personal relationships that could have appeared to influence the work reported in this paper.

## References

[1] A. Benslimane, S. Bouzidi, M. Methia, Displacements and stresses in pressurized thick-walled FGM cylinders: exact and numerical solutions, Int. J. Pres. Ves. Pip. 168 (2018) 219–224.
[2] A. Hadj Mostefa, S. Merdaci, N. Mahmoudi, An overview of functionally graded materials «FGM, in: Proceedings of the Third International Symposium on Materials and Sustainable Development, 2018, pp. 267–278.
[3] C. Evci, M. Gülgeç, Functionally graded hollow cylinder under pressure and thermal loading: effect of material parameters on stress and temperature distributions, Int. J. Eng. Sci. 123 (2018) 92–108.
[4] Y. Anani, G.H. Rahimi, Stress analysis of thick pressure vessel composed of functionally graded incompressible hyperelastic materials, Int. J. Mech. Sci. 104 (2015) 1–7.
[5] L. Gray, T. Kaplan, J. Richardson, G. Paulino, Green's functions and boundary integral analysis for exponentially graded materials: heat conduction, J. Appl. Mech. 70 (4) (2003) 543–549.
[6] L. Guo, N. Noda, Investigation methods for thermal shock crack problems of functionally graded materials–part I: analytical method, J. Therm. Stresses 37 (3) (2014) 292–324.
[7] Y. Zhang, L. Guo, N. Noda, Investigation methods for thermal shock crack problems of functionally graded materials–part II: combined analytical-numerical method, J. Therm. Stresses 37 (3) (2014) 325–339.
[8] L. Marin, Numerical solution of the Cauchy problem for steady-state heat transfer in two-dimensional functionally graded materials, Int. J. Solid Struct. 42 (15) (2005) 4338–4351.
[9] M.H. Babaei, Z. Chen, Transient hyperbolic heat conduction in a functionally graded hollow cylinder, J. Thermophys. Heat Tran. 24 (2) (2010) 325–330.
[10] A.M. Zenkour, Thermoelastic analysis of an annular sandwich disk with metal/ceramic faces and functionally graded core, J. Thermoplast. Compos. Mater. 22 (2) (2009) 163–181.
[11] R. Shirmohammadi, A. Moosaie, Non-Fourier heat conduction in a hollow sphere with periodic surface heat flux, Int. Commun. Heat Mass Tran. 36 (8) (2009) 827–833.
[12] M.H. Ghasemi, S. Hoseinzadeh, S. Memon, A dual-phase-lag (DPL) transient non-Fourier heat transfer analysis of functional graded cylindrical material under axial heat flux, Int. Commun. Heat Mass Tran. 131 (2022) 105858.
[13] M.H. Ghasemi, S. Hoseinzadeh, P.S. Heyns, D.N. Wilke, Numerical Analysis of Non-fourier Heat Transfer in a Solid Cylinder with Dual-Phase-Lag Phenomenon, 2020.
[14] P. Malekzadeh, M. Golbahar Haghighi, Y. Heydarpour, Heat transfer analysis of functionally graded hollow cylinders subjected to an axisymmetric moving boundary heat flux, Numer. Heat Tran., Part A: Applications 61 (8) (2012) 614–632.
[15] P. Malekzadeh, R. Nejati, Non-fourier heat transfer analysis of functionally graded spherical shells under convection-radiation conditions, Journal of Oil, Gas and Petrochemical Technology 1 (1) (2014) 73–86.
[16] N. Tutuncu, B. Temel, A novel approach to stress analysis of pressurized FGM cylinders, disks and spheres, Compos. Struct. 91 (3) (2009) 385–390.

[17] Y. Chen, X. Lin, Elastic analysis for thick cylinders and spherical pressure vessels made of functionally graded materials, Comput. Mater. Sci. 44 (2) (2008) 581–587.
[18] M.Z. Nejad, M. Abedi, M.H. Lotfian, M. Ghannad, Elastic analysis of exponential FGM disks subjected to internal and external pressure, Cent. Eur. J. Eng. 3 (2013) 459–465.
[19] K. Karami, M. Abedi, M. Zamani Nejad, M.H. Lotfian, Elastic analysis of heterogeneous thick-walled spherical pressure vessels with parabolic varying properties, Front. Mech. Eng. 7 (2012) 433–438.
[20] L. You, J. Zhang, X. You, Elastic analysis of internally pressurized thick-walled spherical pressure vessels of functionally graded materials, Int. J. Pres. Ves. Pip. 82 (5) (2005) 347–354.
[21] S.A. Atashipour, R. Sburlati, S.R. Atashipour, Elastic analysis of thick-walled pressurized spherical vessels coated with functionally graded materials, Meccanica 49 (2014) 2965–2978.
[22] Y. Bayat, M. Ghannad, H. Torabi, Analytical and numerical analysis for the FGM thick sphere under combined pressure and temperature loading, Arch. Appl. Mech. 82 (2012) 229–242.
[23] P. Das, M.A. Islam, S. Somadder, M. Hasib, Analytical and numerical analysis of functionally graded (FGM) axisymmetric cylinders under thermo-mechanical loadings, Mater. Today Commun. 33 (2022) 104405.
[24] R. Benchallal, A. Benslimane, O. Bidgoli, D. Hammiche, Analytical solution for rotating cylindrical FGM vessel subjected to thermomechanical loadings, Mater. Today: Proc. 53 (2022) 24–30.
[25] K. Celebi, D. Yarimpabuç, I. Keles, A novel approach to thermal and mechanical stresses in a FGM cylinder with exponentially-varying properties, J. Theor. Appl. Mech. 55 (1) (2017) 343–351.
[26] H.A. Sollund, K. Vedeld, J. Hellesland, Efficient analytical solutions for heated and pressurized multi-layer cylinders, Ocean Eng. 92 (2014) 285–295.
[27] M. Jabbari, S. Sohrabpour, M. Eslami, Mechanical and thermal stresses in a functionally graded hollow cylinder due to radially symmetric loads, Int. J. Pres. Ves. Pip. 79 (7) (2002) 493–497.
[28] T. Sadowski, M. Birsan, D. Pietras, Multilayered and FGM structural elements under mechanical and thermal loads. Part I: comparison of finite elements and analytical models, Arch. Civ. Mech. Eng. 15 (4) (2015) 1180–1192.
[29] K. Abrinia, H. Naee, F. Sadeghi, F. Djavanroodi, New analysis for the FGM thick cylinders under combined pressure and temperature loading, Am. J. Appl. Sci. 5 (7) (2008) 852–859.
[30] Z. Shao, G. Ma, Thermo-mechanical stresses in functionally graded circular hollow cylinder with linearly increasing boundary temperature, Compos. Struct. 83 (3) (2008) 259–265.
[31] D. Sharma, R. Kaur, Thermoelastic analysis of FGM hollow cylinder for variable parameters and temperature distributions using FEM, Nonlinear Eng. 9 (1) (2020) 256–264.
[32] M. Eslami, M. Babaei, R. Poultangari, Thermal and mechanical stresses in a functionally graded thick sphere, Int. J. Pres. Ves. Pip. 82 (7) (2005) 522–527.
[33] A. Eldeeb, Y. Shabana, A. Elsawaf, Investigation of the thermoelastoplastic behaviors of multilayer FGM cylinders, Compos. Struct. 276 (2021) 114523.
[34] M.M. Shahzamanian, A. Shahrjerdi, B.B. Sahari, P.D. Wu, Steady-state thermal analysis of functionally graded rotating disks using finite element and analytical methods, Materials 15 (16) (2022).
[35] M. Meshkini, K. Firoozbakhsh, M. Jabbari, A. SelkGhafari, Asymmetric mechanical and thermal stresses in 2D-FGPPMs hollow cylinder, J. Therm. Stresses 40 (4) (2017) 448–469.
[36] Z. Mazarei, M.Z. Nejad, A. Hadi, Thermo-elasto-plastic analysis of thick-walled spherical pressure vessels made of functionally graded materials, International Journal of Applied Mechanics 8 (4) (2016) 1650054.
[37] M.Z. Nejad, N. Alamzadeh, A. Hadi, Thermoelastoplastic analysis of FGM rotating thick cylindrical pressure vessels in linear elastic-fully plastic condition, Compos. B Eng. 154 (2018) 410–422.
[38] M. Nematollahi, A. Dini, M. Hosseini, Thermo-magnetic analysis of thick-walled spherical pressure vessels made of functionally graded materials, Appl. Math. Mech. 40 (2019) 751–766.
[39] M. Arefi, I. Nahas, Nonlinear electro thermo elastic analysis of a thick spherical functionally graded piezoelectric shell, Compos. Struct. 118 (2014) 510–518.
[40] X. Wang, Z. Wang, T. Zeng, S. Cheng, F. Yang, Exact analytical solution for steady-state heat transfer in functionally graded sandwich slabs with convective-radiative boundary conditions, Compos. Struct. 192 (2018) 379–386.
[41] A.A. Delouei, A. Emamian, S. Karimnejad, H. Sajjadi, D. Jing, Two-dimensional analytical solution for temperature distribution in FG hollow spheres: general thermal boundary conditions, Int. Commun. Heat Mass Tran. 113 (2020) 104531.
[42] A. Amiri Delouei, A. Emamian, S. Karimnejad, H. Sajjadi, A. Tarokh, On 2D asymmetric heat conduction in functionally graded cylindrical segments: a general exact solution, Int. J. Heat Mass Tran. 143 (2019).
[43] A. Amiri Delouei, A. Emamian, S. Karimnejad, H. Sajjadi, A closed-form solution for axisymmetric conduction in a finite functionally graded cylinder, Int. Commun. Heat Mass Tran. 108 (2019).
[44] D. Jing, H. Sajjadi, S. Karimnejad, A. Emamian, A.A. Delouei, Asymmetric conduction in an infinite functionally graded cylinder: two-dimensional exact analytical solution under general boundary conditions, J. Heat Tran. 142 (4) (2020).
[45] S.S. Rathore, V.R. Kar, Thermoelastic eigenfrequency of pre-twisted FG-sandwich straight/curved blades with rotational effect, Struct. Eng. Mech. 86 (4) (2023) 519–533.
[46] S. Kumar, V.R. Kar, Nonlinear fully coupled thermoelastic transient analysis of axial functionally graded composite panel, Mech. Base. Des. Struct. Mach. (2023) 1–30.
[47] S. Kumar, V.R. Kar, Nonlinear fully-coupled thermoelastic analysis of bidirectional porous functionally graded doubly-curved shell panels with optimum material distribution, Mech. Adv. Mater. Struct. (2023) 1–33.
[48] K.K. Joshi, V.R. Kar, Elastoplastic behaviour of multidirectional porous functionally graded panels: a nonlinear FEM approach, Iranian Journal of Science and Technology, Transactions of Mechanical Engineering (2023) 1–23.
[49] S.K. Chaudhary, V.R. Kar, K.K. Shukla, Geometrically nonlinear large-deflection analysis of heated functionally graded composite panels with single and multiple perforations, Mech. Adv. Mater. Struct. (2022) 1–18.
[50] S.K. Chaudhary, V.R. Kar, K.K. Shukla, Flexural behavior of perforated functionally graded composite panels under complex loading conditions: higher-order finite-element approach, J. Aero. Eng. 34 (6) (2021) 04021081.
[51] A. Karakoti, S. Pandey, V.R. Kar, Nonlinear transient analysis of porous P-FGM and S-FGM sandwich plates and shell panels under blast loading and thermal environment, Thin-Walled Struct. 173 (2022) 108985.
[52] Z. Wu, B. Huang, J. Fan, H. Chen, Homotopy based stochastic finite element model updating with correlated static measurement data, Measurement 210 (2023) 112512.
[53] J. Shi, B. Zhao, T. He, L. Tu, X. Lu, H. Xu, Tribology and dynamic characteristics of textured journal-thrust coupled bearing considering thermal and pressure coupled effects, Tribol. Int. 180 (2023) 108292.
[54] Z. Zhu, Y. Liu, G. Gou, W. Gao, J. Chen, Effect of heat input on interfacial characterization of the butter joint of hot-rolling CP-Ti/Q235 bimetallic sheets by Laser + CMT, Sci. Rep. 11 (1) (2021) 10020.
[55] Q. Zhu, J. Chen, G. Gou, H. Chen, P. Li, Ameliorated longitudinal critically refracted—attenuation velocity method for welding residual stress measurement, J. Mater. Process. Technol. 246 (2017) 267–275.
[56] K. Yang, N. Qin, H. Yu, C. Zhou, H. Deng, W. Tian, S. Cai, Z. Wu, J. Guan, Correlating multi-scale structure characteristics to mechanical behavior of Caprinae horn sheaths, J. Mater. Res. Technol. 21 (2022) 2191–2202.
[57] Y. Wang, M. Lou, Y. Wang, C. Fan, C. Tian, X. Qi, Experimental investigation of the effect of rotation rate and current speed on the dynamic response of riserless rotating drill string, Ocean Eng. 280 (2023) 114542.

[58] Z. Fu, B. Yang, M. Shan, T. Li, Z. Zhu, C. Ma, X. Zhang, G. Gou, Z. Wang, W. Gao, Hydrogen embrittlement behavior of SUS301L-MT stainless steel laser-arc hybrid welded joint localized zones, Corrosion Sci. 164 (2020) 108337.
[59] H. Yu, J. Zhang, M. Fang, T. Ma, B. Wang, Z. Zhang, Z. Hu, H. Li, X. Cao, C. Ding, Bio-inspired strip-shaped composite composed of glass fabric and waste selvedge from A. pernyi silk for lightweight and high-impact applications, Compos. Appl. Sci. Manuf. 174 (2023) 107715.
[60] L.-m. Tian, M.-h. Li, L. Li, D.-y. Li, C. Bai, Novel joint for improving the collapse resistance of steel frame structures in column-loss scenarios, Thin-Walled Struct. 182 (2023) 110219.
[61] Y. Mognhod Bezzie, D. Engida Woldemichael, Investigating the graded-index influence on elastic responses of axisymmetric pressurized and heated thick-walled functionally graded material of cylindrical vessel, Forces in Mechanics 7 (2022).
[62] Y. Mognhod Bezzie, D. Engida Woldemichael, Effects of graded-index and Poisson's ratio on elastic-solutions of a pressurized functionally graded material thick-walled cylinder, Forces in Mechanics 4 (2021).
[63] A. Benslimane, R. Benchallal, S. Mammeri, M. Methia, M.A. Khadimallah, Investigation of displacements and stresses in thick-walled FGM cylinder subjected to thermo-mechanical loadings, Int. J. Comput. Methods Eng. Sci. Mech. 22 (2) (2020) 138–149.
[64] L. Xin, J. Xu, Z. Li, Y. Li, A Mori-Tanaka method based theoretical approximation for functionally graded thick wall tube under combined thermal and mechanical loads, J. Therm. Stresses 46 (3) (2023) 229–250.
[65] J.N. Reddy, C.D. Chin, Thermomechanical analysis of functionally graded cylinders and plates, J. Therm. Stresses 21 (6) (1998) 593–626.
[66] A. Najibi, R. Talebitooti, Nonlinear transient thermo-elastic analysis of a 2D-FGM thick hollow finite-length cylinder, Compos. B Eng. 111 (2017) 211–227.
[67] Mahmoud Nemat-Alla, Reduction of thermal stresses by developing two-dimensional functionally graded materials, Int. J. Solid Struct. 40 (26) (2003) 7339–7356.